Copper-doped titania photocatalysts for simultaneous reduction of CO_2 and production of H_2 from aqueous sulfide

Francisco Gonell[a,b], Alberto V. Puga[a], Beatriz Julián-López[b], Hermenegildo García[a], Avelino Corma[a]

[a] *Departament de Química Inorgànica i Orgànica and, Universitat Jaume I, Av. Vicente Sos Baynat, s/n, 12071 Castelló, Spain*
[b] *Instituto Universitario de Tecnología Química CSIC-UPV, Universitat Politècnica de València, Av. De los Naranjos, s/n, 46022 Valencia, Spain*

Keywords

Carbon dioxide, photocatalysis, copper-doped TiO_2, sulfide, wastewater

Abstract

Copper-doped titanium dioxide materials with anatase phase (Cu-TiO_2, atomic Cu contents ranging from 0 to 3% relative to the sum of Cu and Ti), and particle sizes of 12–15 nm, were synthesised by a solvo-thermal method using ethanol as the solvent and small amounts of water to promote the hydrolysis-condensation processes. Diffuse reflectance UV-vis spectroscopy show that the edges of absorption of the titania materials are somewhat shifted to higher wavelengths due to the presence of Cu. X-Ray Photoelectron Spectroscopy (XPS) indicate that Cu(II) is predominant. Photocatalytic CO_2 reduction experiments were performed in aqueous Cu-TiO_2 suspensions under UV-rich light and in the presence of different solutes. Sulfide was found to promote the efficient production of H_2 from water and formic acid from CO_2. The effect of the Cu content on the photoactivity of Cu-TiO_2 was also studied, showing that copper plays a role on the photocatalytic reduction of CO_2.

1. Introduction

Carbon dioxide is an inexpensive and widely available feedstock. Its use for the production of chemicals is doubly beneficial, since in addition to its availability, it would represent a decrease in the carbon footprint for the manufacturing of the particular chemical. Catalytic processes are crucial for improving efficiency and conversion in the use of CO_2 for the manufacture of a wide range of substances, including methanol [1-4], carboxylic acids [1, 4], polycarbonates [1, 4, 5], polylactones [1, 6] or hydrocarbons [1, 4, 7, 8]. As a particularly important matter, the catalytic production of hydrocarbon fuels from CO_2 constitutes a highly desirable strategy for the potential of closing the carbon cycle in future energy schemes. This would in turn contribute to alleviate both our dependence on fossil fuels and the greenhouse effect. Unfortunately, CO_2 is a very stable molecule and its reduction into hydrocarbons is an energy-consuming process. From a sustainability point of view, a source of renewable energy would be required. Thus, one

direction towards the conversion of CO_2 to fuels could be the use of light, most preferably sunlight, as the energy source to promote the reaction. Reduction of CO_2 by H_2 into methane, *i.e.* the Sabatier reaction [9], activated by solar light can be achieved at very high efficiencies on nanoparticulate nickel materials [10] or on various supported metal (especially Ru or Ni) catalysts [11, 12]. A further step in this sense would be the use of H_2O instead of H_2 as the reducing agent, in essence mimicking the activation route of natural photosynthesis. Although more desirable, the latter involves surmounting a considerably high energetic barrier and a complex mechanistic pathway. In recent times, a number of research teams around the world are tackling this issue by designing photocatalysts for the process. The most frequently investigated photocatalysts for these transformations are based on titanium dioxide as the light absorbing semiconductor [13-16], and include one or more co-catalysts, although the focus on other semiconducting materials cannot be neglected [14, 17].

Copper has received attention as a metal with activity in photocatalytic TiO_2 systems for the reduction of CO_2 [13]. By introducing Cu into TiO_2 by various methods, the production of hydrocarbons (such as methanol or methane) from CO_2 at different levels of success has been reported. For example, Cu/TiO_2 materials prepared by impregnation of copper onto a titania support and subsequent calcination have been used to generate methanol photocatalytically from aqueous CO_2 solutions under black light, at production rates as high as 443 μmol g_{cat}^{-1} h^{-1} [18]. Other researchers have reported lower but noticeable methanol yields using similarly prepared photocatalysts and Hg lamp irradiation (10–23 μmol g_{cat}^{-1} h^{-1}) [19, 20]. In gas-phase reactions, the formation of methanol was also reported, but in considerably lower yields (2 nmol g_{cat}^{-1} h^{-1}), being methane the major product formed by Cu/TiO_2 photocatalysis [21]. In contrast, similar materials were found to promote the formation of several hydrocarbons including methane, ethane and ethylene in conjunction with larger amounts of H_2 [22], whereas CO and methane were major products found in a more recent study [23]. A significant degree of discrepancy regarding the identity of the reaction products (in addition to their selectivities and yields) is apparent by considering the aforementioned literature data, although this could be in part due to the different synthetic procedures used for the preparation of the photocatalysts and to the varied irradiation conditions used.

Despite the notable progress in this field of research, there is no clear trend which may allow to conclude on the actual mechanistic route and to gain knowledge on the role of copper on the reaction. Thorough kinetic and in situ spectroscopic studies would provide valuable information on the reaction at the surface of the photocatalyst and may guide future design of more active copper-titania materials. An important issue to focus on is the possible back-reactions of the reduction products on the photocatalyst. For example, it was observed that methanol and formaldehyde, initially formed by a photocatalytic process using Cu(0) powder and TiO_2, were

rapidly consumed by in situ formed Cu/TiO_2 [24]. The simultaneous occurrence of CO_2 reduction and decomposition of the products should result in stationary concentrations reflecting the relative reaction rates. Furthermore, any residual carbon contamination on the photocatalysts, even at low levels, has been shown to seriously interfere with the quantification of CO_2 reduction products and may thus lead to overestimated activities [25].

In this work, photocatalysts based on titanium dioxide containing small amounts of copper ($\leq$ 3% by weight) have been prepared by a solvo-thermal method. This procedure leads to Cu-doped anatase TiO_2. Copper is mostly within the TiO_2 framework, thus forming isolated copper sites, as opposed to the most commonly used Cu-impregnated materials. The use of these materials for the photocatalytic reduction of CO_2 in aqueous suspensions has been investigated. The effect of copper content and of additional solutes on the efficiency of the process has been studied. Sulfide, which is a common and undesirable water pollutant [26, 27], has been selected as an efficient sacrificial electron-donating solute. In addition to the sulfide anion, its conjugated acid hydrogen sulfide is a large scale by-product in petrochemical processing [28, 29] (where it is converted to elemental sulfur for disposal), and uses thereof are intensively sought as a desirable strategy for its valorisation as a feedstock [30]. The possibility of using sulfide species as sacrificial electron donors for the photocatalytic production of fuels has been extensively studied mostly on metal sulfide semiconductors, although these processes often require additional solutes such as sulfite to prevent photocorrosion [27-29]. In contrast, the system presented here relies on a stable copper-titania photocatalyst which can remove aqueous sulfide, without the need of additives, with simultaneous production of H_2 and reduction of CO_2.

2. Results and discussion

2.1 Synthesis of the photocatalysts

Nanoparticulate copper-doped TiO_2 materials have been prepared by a solvo-thermal method based on the hydrolysis-condensation of a titanium alkoxyde (2-propoxide) using ethanol as the solvent and a small amount of water in order to promote the hydrolysis reaction. Copper acetate was used as the Cu precursor, and acetylacetone was added in order to form the corresponding complex. Then, the solubility of the metallic cation increases and the availability of copper to be incorporated into the nascent TiO_2 lattice is kinetically controlled. The result is the effective introduction of Cu in the as-prepared Cu-TiO_2 materials. A range of these samples, designated here as ^{AP}XCu-TiO_2 (X = 0.5, 1.0, 1.5, 2.0 and 3.0, where X is the atomic percentage of Cu

relative to the sum of Cu and Ti, and ^{AP} stands for "as-prepared") were synthesized in this study, in addition to an analogous material without copper (X = 0.0).

The thermal behaviour of ^{AP}3.0Cu-TiO_2 was studied by thermogravimetric analysis (TGA, see supplementary data) as a representative example. The thermal curves of this as-prepared material exhibit two steps: a first weight loss was recorded at around 80^{o}C (most likely due to desorption of both water and residual solvents), and a second one at around 275 ^{o}C (probably related to the combustion of organic moieties from acetate and acetylacetone derivatives, and corresponding to *ca.* 10% organic matter by weight). According to the TGA results, the ^{AP}XCu-TiO_2 materials were calcined in air at 500^{o}C in order to remove any possible organic matter, thus yielding the final XCu-TiO_2 (X = 0.0, 0.5, 1.0, 1.5, 2.0 and 3.0, see above, 0.0Cu-TiO_2 designated herein also as TiO_2 for simplicity).

2.2 Characterisation of the photocatalysts

All the prepared Cu-doped titanium dioxide materials were characterized by X-ray diffraction. Figure 1 (a) and (b) show the X-ray diffraction patterns of the as-prepared and calcined materials, respectively. The as-prepared samples show broad diffraction peaks associated to nanocrystalline TiO_2 anatase phase (JCPDS 21-1272). The crystallite size calculated using the Scherrer equation is around 7 nm for all samples (see Table 1 for more details, and supplementary data for confirmation by transmission electron microscopy). After annealing at 500 $^{\circ}$C the anatase phase is preserved, but the peaks become sharper as a consequence of the crystallisation of any amorphous material remaining, diminution of lattice defects and crystal growth. The Scherrer calculations indicate larger, but still nanometric, crystallite sizes of around 13 nm (Table 1). In contrast to the as-synthetized materials, the patterns of the annealed Cu-doped samples show a shift towards lower 2θ values in comparison to the TiO_2 reference. This is the case for the diffraction associated with the (101) planes at *ca*. 25.3 ° (see Figure 1, bottom right). Taking into account the ionic radii of the copper and titanium ions in octahedral coordination (Cu^{2+}: 73 pm and Ti^{4+}: 60.5 pm) [31], the shift agrees with a substitutional solid solution in which Cu ions would occupy the Ti sites in the TiO_2 lattice. No peaks from CuO or Cu_2O phases were observed.

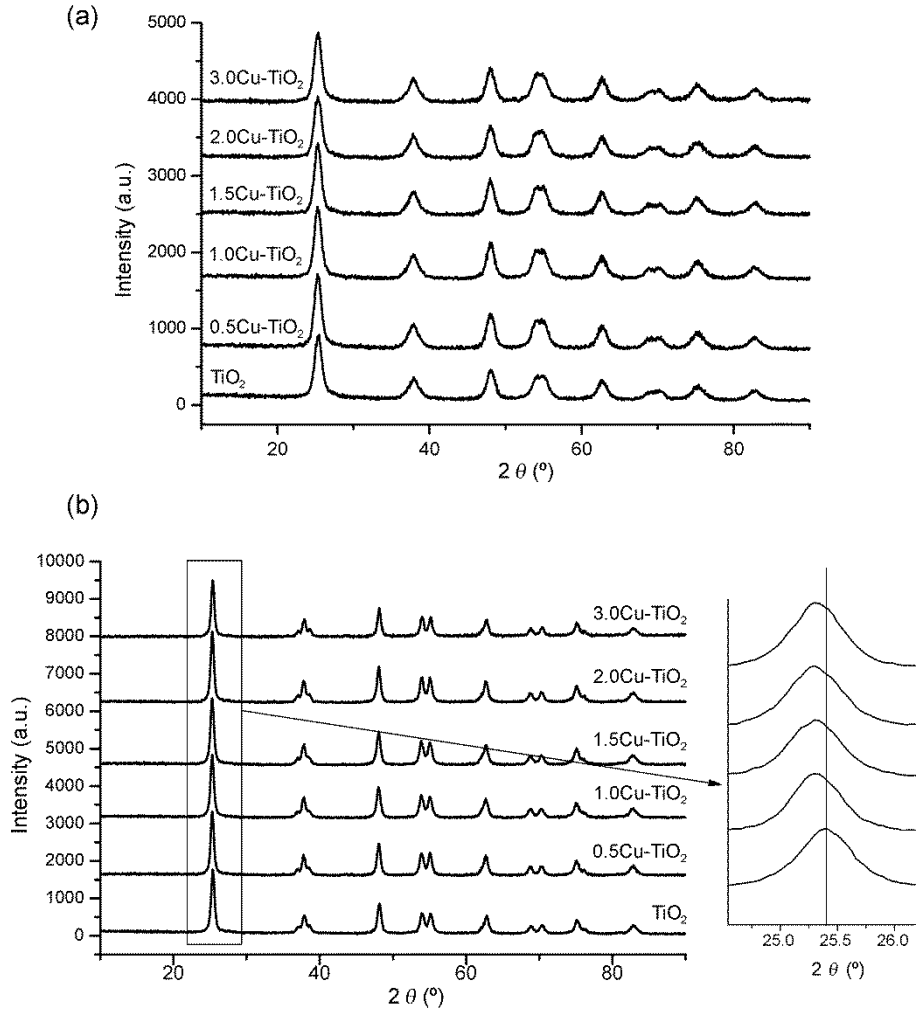

Figure 1. X-ray diffraction patterns of ^{AP}XCu-TiO_2 (before calcination, (a)) and XCu-TiO_2 (after calcination in air at 500 °C, (b)) samples. The inset on the bottom-right side shows the shift of the (101) anatase diffraction for different copper contents in XCu-TiO_2 materials.

Figure 2 shows the Raman spectra of the Cu-TiO_2 samples. All the signals recorded correspond to the anatase phase, in good agreement with the XRD analysis of calcined samples. The spectra are characterized by intense bands at 144 cm^{-1}, three less intense bands at 396, 517, 639 cm^{-1} and a shoulder at 196 cm^{-1}, which correspond to the TiO_2 vibrational modes of E_g, B_{1g}, A_{1g}, B_{1g}, and E_g, symmetries, respectively [32]. As in the case of XRD, the presence of CuO or Cu_2O could not be detected by Raman, although that possibility cannot be completely ruled on the bases of these techniques due to the low copper contents of these materials.

Table 1. Crystallite sizes, BET surface areas and band gaps of Cu-TiO_2 samples.

sample	crystallite size (nm) as-prepared[a,b)]	crystallite size (nm) after calcination[a)]	S_{BET} (m^2/g)[c,d)]	band gap (eV)[d,e)]
3.0Cu-TiO_2	6.6	13.1	37.2	2.98
2.0Cu-TiO_2	6.6	13.5	38.3	3.06
1.5Cu-TiO_2	6.4	12.9	49.2	3.10
1.0Cu-TiO_2	6.8	12.9	46.1	3.12
0.5Cu-TiO_2	6.9	14.1	30.2	3.14
TiO_2	6.6	12.9	45.7	3.17

[a)] Calculated from XRD data using the Scherrer equation. [b)] Measured for as-prepared materials (^{AP}XCu-TiO_2) before calcination. [c)] Specific surface areas determined by N_2 adsorption-desorption. [d)] Measured for XCu-TiO_2 (after calcination). [e)] Calculated from UV-vis absorption data by using the Kubelka-Munk function.

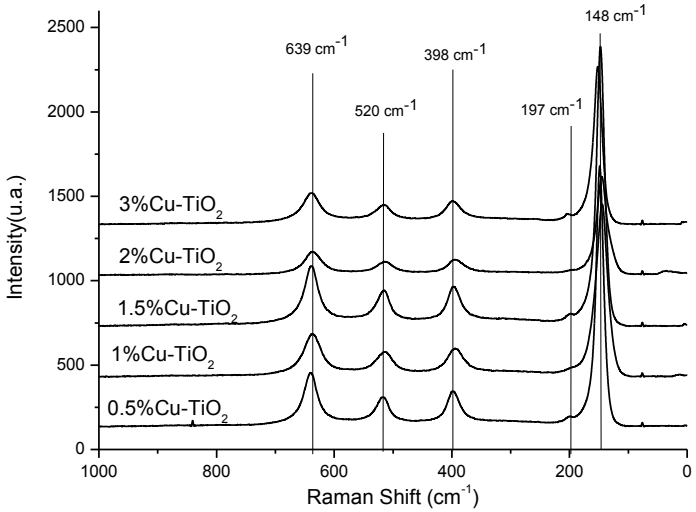

Figure 2. Raman spectra of XCu-TiO_2 samples (X = 0.5, 1.0, 1.5, 2.0 and 3.0).

The field emission gun scanning electron microscopy (FEG-SEM) images of the annealed samples (Figure 3) reveal that the Cu-TiO_2 materials were composed by aggregates of small nanocrystals. Therefore, a more detailed analysis by transmission electron microscopy (TEM) was also performed.

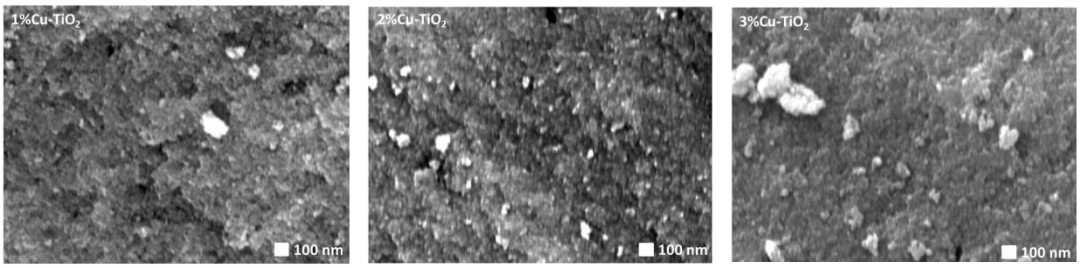

Figure 3. FEG-SEM micrographs of *X*Cu-TiO_2 samples (*X* = 0.5, 1.0, 1.5, 2.0 and 3.0).

Characterisation of the morphology and structure of 3.0Cu-TiO_2 by high-resolution transmission electron microscopy (HR-TEM, see Figure 4) confirmed that this material consisted of agglomerates of quasi-spherical nanocrystalline particles with a size of 10–15 nm, which fits well with the crystal size calculated by the Scherrer equation (see above). The planar distances of the crystalline particles measured from the HR-TEM images correspond well with the distance of anatase planes (0.35 nm). No segregated copper species or particles were detected for any copper-doped samples. Furthermore, elemental mapping performed by energy dispersive X-ray (EDX) spectroscopy under scanning transmission mode, indicate a good dispersion of copper throughout the solid (see supplementary data). These observations suggest that an effective solid solution is obtained, in good agreement with XRD and Raman data.

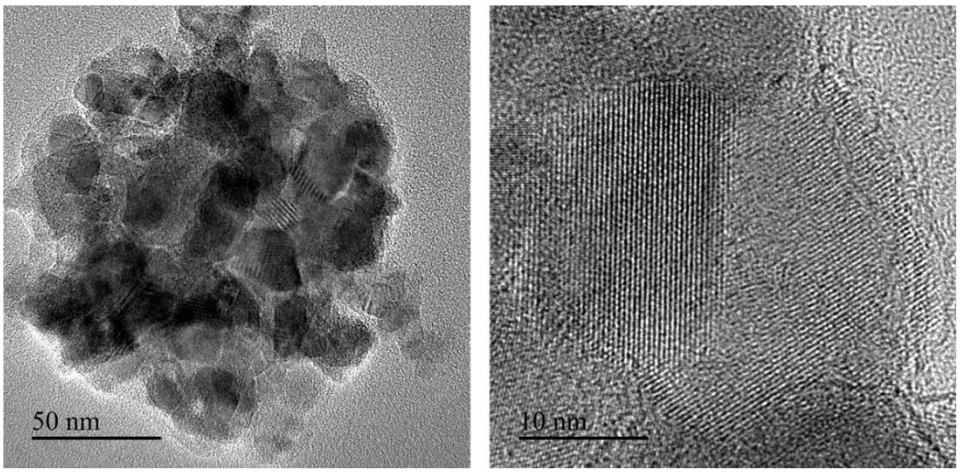

Figure 4. HR-TEM micrographs of 3.0Cu-TiO_2.

Textural properties were studied by N_2 adsorption-desorption showing a BET surface area around 30–50 m^2/g with no dependence on the Cu content. As can be expected, when crystal sizes estimated by the Scherrer equation decrease, BET surface areas increase.

Figure 5 shows the diffuse reflectance UV-vis (DRUV-vis) spectra of the different Cu-doped samples. The absorption edge shifts towards the visible region upon addition of Cu, and the band gap decreases from 3.17 to 2.98 eV when the doping level is increased from 0 to 3%. The band gap shift can be attributed to the presence of Cu ions in the TiO_2 matrix introducing new energy levels to the intra-band space. The broad band between 600 and 800 nm corresponds to d-d transitions of Cu^{2+} in O_h symmetry with a tetragonal distortion. No bands corresponding to metallic copper were observed at 580-590 nm [33-36].

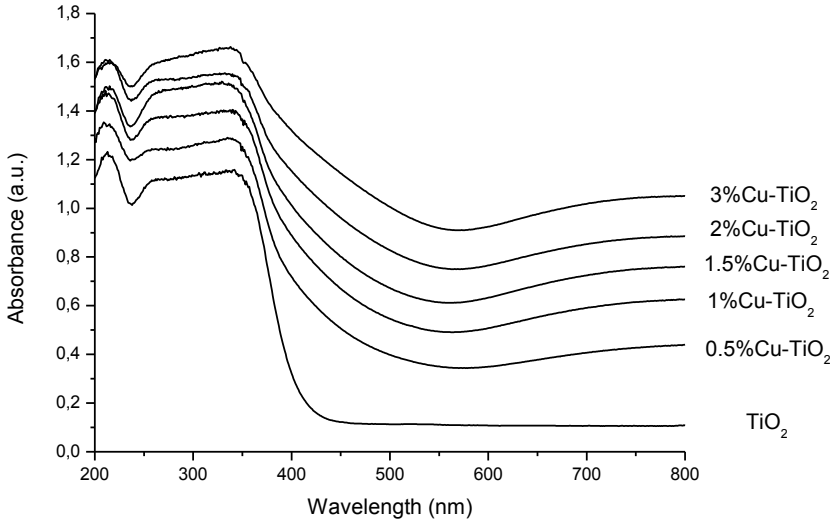

Figure 5. DRUV-vis spectra of *X*Cu-TiO_2.

The newly synthesised copper-doped titania materials have also been studied by X-ray Photoelectron Spectroscopy (XPS). Peak positions for Cu 2p3/2 and Ti 2p3/2 photoelectrons are listed in Table 2. Data for titania-supported copper catalysts prepared by impregnation methods (^{IM}3.0Cu/TiO_2, where the nominal weight percentage of copper is 3.0%) are also included for comparison. The positions of the Cu 2p3/2 photoelectron energies are different depending on the synthetic method and on the Cu content in the case of copper-doped TiO_2 samples. In either case, only one component for such bands could be observed, indicating that Cu is present in only one oxidation state. Bands for the materials prepared by impregnation are found at higher binding energies than for the doped counterparts. For example, ^{IM}3.0Cu/TiO_2 and 3.0Cu-TiO_2 exhibit their Cu 2p3/2 peaks at 935.4 and 934.5 eV, respectively. In principle, this suggests that the Cu-impregnated samples have more positive charge density on Cu (probably as CuO) than when in the lattice of TiO_2. Regarding the doped samples, a decrease in binding energy is observed for decreasing copper contents. This can indicate that the positive charge density of Cu ions decreases as its population in the titania matrix decreases. However, it should be pointed

out that Cu 2p3/2 signals were weak, due to the low copper contents, and the uncertainties of the corresponding binding energies might be significant. Furthermore, copper tends to reduce under the X-ray beam and thus, short accumulations were performed during the measurements.

Table 2. XPS data for ^{IM}3.0Cu/TiO_2 (Cu-impregnated) and *X*Cu-TiO_2 (Cu-doped) samples.

photocatalyst	Cu 2p3/2 binding energy/eV
^{IM}3.0Cu/TiO_2	935.3
3.0Cu-TiO_2	934.5
2.0Cu-TiO_2	933.6
1.5Cu-TiO_2	934.1
1.0Cu-TiO_2	932.3
0.5Cu-TiO_2	932.7

2.3 Photocatalytic CO_2 reduction on aqueous Cu-TiO_2 suspensions

The Cu-TiO_2 materials prepared in this work have been tested as photocatalysts for the CO_2 reduction in aqueous media and under light irradiation, from a UV-rich mercury lamp unless otherwise specified. The reactions were performed in the presence of different sacrificial electron donors in order to facilitate the activation of the otherwise essentially unreactive CO_2 substrate. The detected products mainly included H_2, CO and CH_4 in the gaseous phases, and formic acid in the liquid phases. Production data for most of the identified products, as analysed from both gaseous and liquid phases, are listed in Table 3.

Table 3. Product yields for the photocatalytic CO_2 reduction under UV-rich light on 3.0Cu-TiO_2.[a)]

			Production rate/μmol g_{cat}^{-1} h^{-1}			
			Gas phase			Liquid phase
Entry	Solute	Photocatalyst	CH_4	CO	H_2	HCOOH
1	-[b)]	3.0Cu-TiO_2	-	-	-	-
2	-	3.0Cu-TiO_2	0.3	0.3	0.6	-
3	NaOH (100 mM)	3.0Cu-TiO_2	-	0.3	-	-
4	NaCl (500 mM)	3.0Cu-TiO_2	-	0.8	1.8	-
5	NaBr (500 mM)	3.0Cu-TiO_2	-	0.5	0.7	-
6	Na_2S (13 mM)	3.0Cu-TiO_2	-	2.8	209.4	25.7
7	Na_2S (13 mM)	^{IM}3.0Cu/TiO_2	-	0.5	175.9	-
8	-	^{IM}3.0Cu/TiO_2	-	-	-	-

[a)] Reaction conditions: Stirred suspensions of the photocatalyst (25 mg) in water (25 mL) in the presence of the specified amounts of sacrificial electron donor (solute) were irradiated with a Hg lamp (125 W) under a CO_2 atmosphere (1.4 bar) at 25 °C for 15 h; hyphens denote figures lower than the corresponding detection limits. [b)] Performed under Ar atmosphere (1.4 bar), without CO_2.

It can be seen in Table 3 that no gas phase products were formed when the reaction was performed in the absence of electron donors and under Ar instead of CO_2 (entry 1) The fact that no H_2 was produced rules out the influence of the water splitting reaction under the irradiation conditions used. Also in the absence of added solutes, but under CO_2 pressure, small amounts of products (0.3 μmol g_{cat}^{-1} h^{-1} for CO or CH_4, marginally above their detection limits, see Table 3, entry 2) were detected. Then, a series of solutes were tested, seeking the conversion of CO_2 under irradiated aqueous suspensions of 3.0Cu-TiO_2. The possible benefits of hydroxide salts, that is, increasing the amount of the CO_2 substrate in the form of carbonate and bicarbonate anions in solution, were investigated by using NaOH as the added solute. Unfortunately, no liquid phase products were formed and only traces of CO were detected (Table 3, entry 3). Halide salts (Cl^- and Br^-) were also tested, resulting in the production of minor amounts of CO and H_2, although the yields were not relevant, and no liquid phase products such as formic acid or methanol were found (Table 3, entries 4 and 5, respectively). Thus, neither hydroxides nor halides were further studied. Being theoretically more efficient electron donors, oxidisable sulfur-based anions were then considered. It was clearly observed that the presence of dissolved

sulfide (Na_2S) led to the formation of significant amounts of H_2, HCO_2H and low, but non-negligible, levels of CO (Table 3, entry 6). These results suggest that S^{2-} is a suitable electron donor for water and CO_2 reduction reactions under UV-rich irradiation on Cu-TiO_2 photocatalysts. The higher amounts (209.4 μmol g_{cat}^{-1} h^{-1}) of H_2 formed reveal that water was more easily reduced, thus competing with the less energetically favourable activation of CO_2. However, it should be noted that the formation of CO_2 reduction products (HCO_2H and CO) on 3.0Cu-TiO_2 proceeds at noticeably high rates, in excess of 25 μmol g_{cat}^{-1} h^{-1}. These yields are higher than some of the most efficient systems reported [19, 20, 37]. In addition, the activity of the newly prepared Cu-TiO_2 photocatalysts took place in the presence of small amounts of sulfide as the only sacrificial electron donor, without the need for additional reducing agents, as observed elsewhere for ZnS photocatalysts [38].

Copper doping within the titania lattice was anticipated as an important factor regarding the photocatalytic activity of the material, since a homogenous distribution would result in both the preferential formation of isolated copper atoms and the efficient transfer of the photogenerated charges from titania. Such isolated copper atoms should become more ubiquitous and readily accesible active sites than for impregnated samples, whereby copper occurs as particles or aggregates. In order to prove the concept, the photoactivity of ^{IM}3.0Cu/TiO_2 was tested (Table 3, entry 7). It can be observed that the formation of CO_2 reduction products was almost completely supressed when using the Cu-impregnated material, since only a small amount of CO was produced. Formic acid was not formed, in contrast to the case of 3.0Cu-TiO_2 prepared by the solvo-thermal procedure. The photocatalytic activity of ^{IM}3.0Cu/TiO_2 in the presence of sulfide led uniquely to the formation of H_2 at a rate (175.9 μmol g_{cat}^{-1} h^{-1}) which somewhat lower than for the doped sample. Furthermore, the Cu-impregnated material did not exhibit any photoactivity in the absence of added solutes (Table 3, entry 8), in contrast to the Cu-doped sample, which promotes the slow but measurable formation of CO_2 reduction products and H_2 (Table 3, entry 2).

2.4 Effect of copper content

Copper-doped titania photocatalysts containing different amounts of doping metal (*X*Cu-TiO_2, *X* = 0.0, 0.5, 1.0, 1.5, 2.0 and 3.0) were then tested for the reduction of CO_2 in the presence of sulfide and under UV irradiation. The production rates of HCO_2H, H_2 and CO are plotted *vs.* copper content in Figure 6. In all cases, H_2 was the major product found, followed by HCO_2H. Under analogous conditions, photoactivity is low for Cu contents below 1%. Pure titania prepared by the same solvo-thermal method also catalyses the formation of certain amounts of H_2 and formic acid under UV-rich light, whereas a small amount (0.5%) of Cu dopant in the

material leads to an increase in H_2 yields and a slight decrease in formic acid production. The amounts of photogenerated products (especially those of H_2) experience a clear increase for higher (≥ 1%) Cu doping levels (see Figure 6). Regarding H_2 production rates, a maximum is observed for 2.0Cu-TiO_2 (313.2 μmol g_{cat}^{-1} h^{-1}). The case of formic acid is peculiar, since its production rates decrease as the titania materials become more enriched in Cu, up to a minimum (3.0 μmol g_{cat}^{-1} h^{-1}) at 1.5%, and then increase again for higher Cu doping levels, reaching values as high as 25.7 μmol g_{cat}^{-1} h^{-1} in the case of 3.0Cu-TiO_2. The yields of CO were moderate for all materials, although they increased with increasing copper contents (2.8 μmol g_{cat}^{-1} h^{-1} when using 3.0Cu-TiO_2).

In summary, it appears that the presence of copper plays a key role in these photocatalysts by affecting their activity and selectivity. The material containing more copper (3.0Cu-Ti) exhibits considerable H_2 production and enhanced selectivity towards formic acid. Furthermore, it should be stressed again that the local environment of copper is also crucial, since Cu-doped samples promote the photocatalytic CO_2 reduction much more efficiently than Cu-impregnated samples (see Table 3).

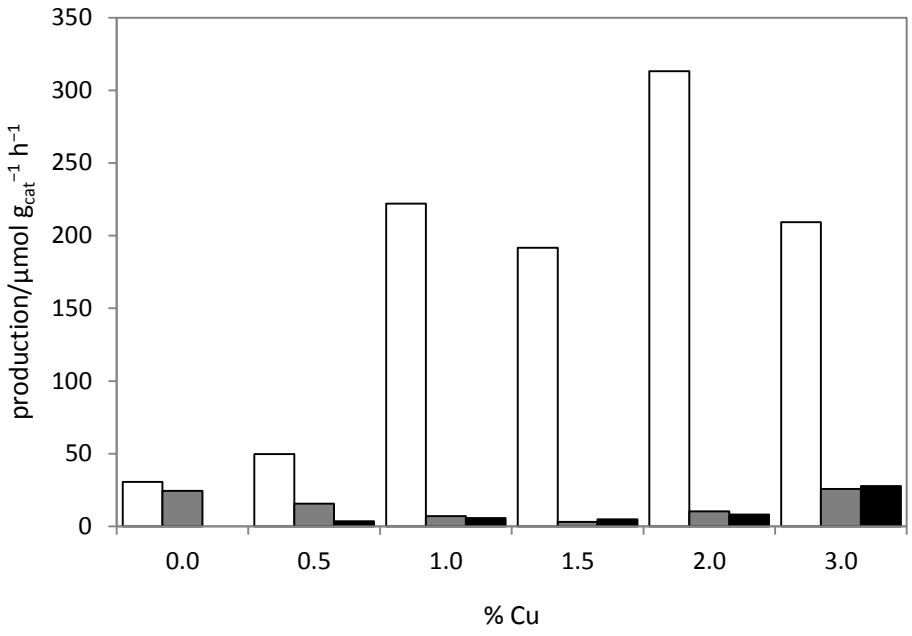

Figure 6. Influence of copper content in *X*Cu-TiO_2 on product formation from the CO_2 reduction in irradiated aqueous suspensions. Experimental conditions: catalyst (25 mg) in water (25 mL) containing Na_2S (13 mM) under a CO_2 atmosphere (1.4 bar) at 25 °C for 15 h; Hg lamp, irradiance ≈ 1.5 kW m^{-2}. White bars: H_2; grey bars: HCO_2H; black bars: CO (due to the low CO amounts, these values are magnified ten-fold for clarity).

2.5 Sulfur abatement and separation

The fate of sulfide as electron donor was also investigated. For reaction catalysed by Cu-doped titania materials, off-white insoluble solid products were observed on top of the solutions at the end of the irradiations. After sedimentation of the photocatalyst, these solids could be isolated by a simple decantation/skimming procedure (or by extraction using tetrachloroethylene for quantitation purposes, as detailed in the Experimental section) and analysed, revealing that they were mainly composed of elemental sulfur (S_n). In the case of the reaction photocatalysed by 2.0Cu-TiO_2, the amount of S_n produced (*ca*. 328 μmol g_{cat}^{-1} h^{-1}) was consistent with the reduction products formed (324.4 μmol g_{cat}^{-1} h^{-1}) according to the expected stoichiometries (equations 1–3 and equation 4 for reduction and oxidation processes, respectively).

$$2\ H^+ + 2\ e^-(\text{Cu-TiO}_2) \rightarrow H_2 \quad (1)$$

$$CO_2 + 2\ e^-(\text{Cu-TiO}_2) + 2\ H^+ \rightarrow HCO_2H \quad (2)$$

$$CO_2 + 2\ e^-(\text{Cu-TiO}_2) + 2\ H^+ \rightarrow CO + H_2O \quad (3)$$

$$S^{2-} + 2\ h^+(\text{Cu-TiO}_2) \rightarrow {}^1\!/_n\ S_n \quad (4)$$

The photocatalytic system reported herein allows reduction of CO_2 at significant rates and concomitant production of H_2 from water, whereas sulfide is transformed into elemental sulfur, which can be separated from the aqueous suspension by only using physical methods. This proves to be advantageous as compared to other methods by which sulfide is transformed to sulfate and/or thiosulfate [27, 29]. Thus, a process combining the abatement of sulfide contamination in waste water and the light-promoted reduction of water and CO_2 can be envisaged using Cu-doped titania photocatalysts. Considering that sulfides are noxious pollutants in wastewaters, the present process represents a valorisation of this undesirable chemical by generating fuels and allowing the recovery of valuable elemental sulfur.

3. Conclusions

The synthesis of nanoparticulate copper-doped titania photocatalysts can be achieved by a solvo-thermal method using ethanol as the solvent. The addition of small amounts of water induced the controlled hydrolysis-condensation of titanium isopropoxide in the presence of Cu^{2+}, thus giving rise to Cu-TiO_2 solids composed of small anatase crystallites (12–15 nm in diameter). Copper is incorporated the bulk of the crystalline titania matrix, thus resulting in the substitution of Ti(IV) atoms with Cu(II), with certain expansion of the anatase lattice, as

evidenced by a shift in the X-ray diffraction angles of its (101) planes. The band gaps of the materials experience a slight but steady decrease with increasing Cu content, a phenomenon which confirms its homogeneous distribution throughout the structure. The effect of copper doping on the photocatalytic activity of these Cu-TiO_2 materials in the UV-induced reduction of CO_2 has been studied. Based on thorough analyses of reaction products and their yields, we have shown that copper-doped titania has the potential to enhance the formation of formic acid and CO, in the presence of sulfide as an electron donor. In addition, concomitant and significant production of H_2 (in excess of 300 $\mu mol\ g_{cat}^{-1}\ h^{-1}$) was achieved. Given the simultaneous reduction of H_2O and CO_2 and the consumption of sulfide, a highly undesirable noxious and toxic pollutant, this finding is promising for combining fuel generation and environmental remediation in a clean and efficient light-activated process.

4. Experimental Section

Materials: Copper(II) acetate monohydrate (≥ 99%), copper(II) nitrate hemi(pentahydrate) (≥ 98%), titanium(IV) isopropoxide, acetylacetone (≥ 99%), sodium sulfide (99%) and tetrachloroethylene (99%) were supplied by Sigma-Aldrich. Sodium hydroxide (pellets, 98%) was supplied by VWR. Titanium dioxide (Aeroxide® P25) was kindly supplied by Evonik Degussa. Carbon dioxide (≥ 99,995%) and argon (≥ 99,995%) were supplied by Abelló Linde. Absolute ethanol (Multisolvent® HPLC grade) was supplied by Scharlau.

Synthesis: The copper-doped materials with 0.0, 0.5, 1.0, 1.5, 2.0 and 3.0% Cu molar ratios (relative to the sum of Cu and Ti; *X*Cu-TiO_2, where X = 0.0, 0.5, 1.0, 1.5, 2.0 and 3.0, respectively) were prepared following a solvothermal methodology. Briefly, the proper amounts of $Ti(OiPr)_4$ and $Cu(OAc)_2 \cdot H_2O$ for obtaining 1 g of the oxide were dissolved in a mixture of ethanol (50 mL) and water (0.9 mL). Acetylacetone (acac) was added in a metal/acac ratio of 1:2 and stirred for 15 min. Then, the solution was transferred into a 125 mL teflon-lined autoclave and heated to 180 °C for 24 h. The products were washed with ethanol several times and collected by centrifugation and dried to yield the as-prepared (^{AP}XCu-TiO_2). Finally, the air-dried powders were annealed in air at 500 °C for 2 h, giving rise to the final *X*Cu-TiO_2 materials.

The copper-impregnated sample (^{IM}3.0Cu/TiO_2) was prepared by an incipient wetness method. A solution of $Cu[NO_3]_2 \cdot 2½H_2O$ (57.0 mg) in water (1.1 mL) was slowly added to ground Aeroxide® P25 TiO_2 (519 mg) to obtain a homogeneous slurry, which was dried in a dessicator

(*ca*. 10 mbar) at room temperature for 1 h. The resulting pale blue powder was calcined at increasing temperatures (up to 150 °C at 3 °C min^{-1}, then maintained for 2 h, and finally up to 500 °C at 5 °C min^{-1} and held at that temperature for 0.5 h). After cooling down to room temperature and grinding on a mortar, $^{IM}3.0Cu/TiO_2$ was obtained as a green-grey solid.

Characterization: XRD measurements were performed by means of a PANalytical Cubix'Pro diffractometer equipped with an X'Celerator detector and automatic divergence and reception slits using Cu-Kα radiation (0.154056 nm). The mean size of the ordered (crystalline) domains (*d*) was estimated using the Scherrer equation. The equation can be written as $d = \frac{0.9\,\lambda}{\beta\,cos\theta}$, where λ is the X-ray wavelength, β is the line broadening at half the maximum intensity (FWHM), after subtracting the instrumental line broadening, in radians, and θ is the Bragg angle. Raman spectra were recorded with a spectral window of 1000–100 cm^{-1} on a Jasco NRS-3100 laser Raman spec-trophotometer (exc = 785 nm). N_2 Adsorption–desorption isotherms were collected on a Micromeritics Gemini V gas adsorption analyzer at 77 K, after degassing the samples at 423 K overnight in a Micromeritics Flow prep 060 system with nitrogen flux gas. The BET surface areas were calculated from the adsorption branch of the isotherm according to the BJH method. DRUV-vis absorption spectra were carried out with a CARY 500 SCAN VARIAN spectrophotometer in the 300–800 nm range. Scanning electron micrographs of the samples were taken with a field emission gun scanning electron microscope (FEG-SEM) model JEOL 7001F, equipped with a spectrometer of energy dispersion of X-ray (EDX) from Oxford instruments by using the following operational parameters: acceleration voltage 20 kV, measuring time 100 s, working distance 25 mm, counting rate 1.2 kcps. The characterization by HRTEM was carried out in a Jem-2100 LaB_6 (Jeol) microscope, at an accelerating voltage of 200 kV, coupled with an Inca Energy TEM 200 (Oxford) energy dispersive X-ray (EDX) spectroscopy. Thermogravimetric analysis (TGA) was performed using a Mettler Toledo TGA/SDATA851e thermo-balance under air from room temperature to 800 °C. X-ray photoelectron spectra were collected on a SPECS spectrometer equipped with a 150-MCD-9 detector and using a non-monochromatic Al Kα (1486.6 eV) X-ray source. Spectra were recorded at 175 °C, using an analyzer pass energy of 30 eV, an X-ray power of 50 W and under an operating pressure of 10^{-9} mbar. During data processing of the XPS spectra, binding energy (BE) values were referenced to the C1s signal (284.6 eV). Spectra treatment has been performed using the CASA software.

Photocatalytic reactions: In a typical experiment, the photocatalyst powder (25 mg) was suspended in water (25 mL) by sonication for 15 min. For some experiments, a certain amount (generally, 13 mM) of a sacrificial electron donor (*e.g.* Na_2S) was dissolved in the aqueous liquid. The resulting suspension was then transferred to a cylindrical quartz reactor (diameter ≈

44 mm, volume ≈ 50 mL, equipped with a gas inlet valve, a gas outlet valve and a pressure gauge) and purged with CO_2 (5 mL min^{-1} for 15 min, and then pressurized-depressurised to 1.4 bar for five cycles); the reactor was finally loaded with the desired gas (1.4 bar) and tightly closed. The suspension was stirred (500 min^{-1}) and irradiated with either a medium pressure Hg lamp (125 W, irradiance ≈ 1.5 kW m^{-2}) for 15 h; the reactor vessel was kept in a water bath at *ca*. 25 °C throughout the experiment. After the light had been switched off, the reaction mixtures were stirred until the pressure reading had stabilised. Two different gaseous samples were taken: (*g1*) a 2.5 cm^3 sample which was injected on a two-channel chromatograph (Agilent 490 Micro GC, carrier gas: Ar) equipped with thermal conductivity detectors (TCD), and a MolSieve 5Å column (first channel) for the quantification of H_2 and CO, and a PoraPLOT Q column (second channel) for the quantification of CO_2 and CH_4; and (*g2*) a 50 cm^3 sample, which was then taken by collecting the entire amount of headspace gas in the reactor and further flushing with more CO_2 and injected on a three-channel chromatographic system (Varian 450-GC Rapid Refinery Gas Analyser) equipped with one TCD for the quantification of H_2 (first channel), one TCD for the quantification of CO_2 and CO (second channel), and one flame ionisation detector (FID) for the quantification of CH_4 (third channel), using Ar (first channel) and He (second and third channels) as the carrier gases. The amounts of H_2, CH_4 and CO were averaged over the figures obtained by analyses of both gaseous samples (*g1* and *g2*), which agreed within a standard deviation of *ca*. 4%. Moreover, two different liquid samples, obtained from a centrifuged and decanted aliquot of the final suspension, were analysed as follows: (*l1*) a *ca.* 0.5 g sample was diluted with ultrapure water (*ca.* 4.5 g), acidified by addition of a 1.4 M aqueous H_2SO_4 solution (*ca.* 0.015 g), and analysed by liquid chromatography on a Coregel 87H column (Waters 1525 Binary HPLC Pump, injection volume = 10 μL, column temperature = 70 °C, eluent: 4 mM aqueous H_2SO_4, flow rate = 0.7 mL min^{-1}) and a refractive index detector (Waters 2410) for the quantification of formic acid; and (*l2*) a liquid sample was injected without any further treatment (actual injection volume = 1 μL) on a gas chromatograph (Agilent Technologies 7890A GC System) equipped with a DB-wax column (carrier gas: He, flow rate = 1 mL min^{-1}) and a FID, aiming at the detection of methanol.

Sulfur separation after irradiations: At the end of the photocatalytic reactions performed in the presence of Na_2S, an off-white solid floating on the liquid was observed. After allowing the suspensions to settle, the solid remained on top and could be separated by skimming. For a quantitative analysis of such solid, an extraction was performed. In a typical separation, the final suspension from the reaction catalysed by 2.0Cu-TiO_2 was mixed with tetrachloroethylene (10 mL) and the resulting colourless bottom phase further washed using the same solvent (3 × 2 mL). The combined organic extracts were dried by mixing with anhydrous magnesium sulfate and subsequent separation by filtration. The solvent was removed under reduced pressure on a

rotary evaporator, yielding a pale yellow solid (4.0 mg; corresponding mainly to elemental sulfur according to elemental analysis; 0.12 mmol).

Acknowledgments

Financial support by the Spanish Ministry of Economy and Competitiveness (Severo Ochoa and CTQ2012-32315) is gratefully acknowledged. F.G. and B.J.-L. are thankful for financial support from Spanish Government (AP2010-2748 PhD grant and MAT2011-27008 project) and Jaume I University (P1 1B2014-21 project). SCIC from Jaume I University and Servicio de Microscopía Electrónica at Universitat Politècnica de València are also acknowledged for instrumental facilities. A.V.P. is grateful to both the Consejo Superior de Investigaciones Cientificas (CSIC) and the European Social Fund (ESF) for a JAE-Doc postdoctoral grant.

References

[1] M. Aresta, A. Dibenedetto, A. Angelini, Chem. Rev., 114 (2014) 1709-1742.
[2] J. Graciani, K. Mudiyanselage, F. Xu, A.E. Baber, J. Evans, S.D. Senanayake, D.J. Stacchiola, P. Liu, J. Hrbek, J. Fernandez Sanz, J.A. Rodriguez, Science, 345 (2014) 546-550.
[3] F. Studt, I. Sharafutdinov, F. Abild-Pedersen, C.F. Elkjaer, J.S. Hummelshøj, S. Dahl, I. Chorkendorff, J.K. Nørskov, Nat. Chem., 6 (2014) 320-324.
[4] M. Mikkelsen, M. Jørgensen, F.C. Krebs, Energy Environ. Sci., 3 (2010) 43-81.
[5] D.J. Darensbourg, Chem. Rev., 107 (2007) 2388-2410.
[6] R. Nakano, S. Ito, K. Nozaki, Nat. Chem., 6 (2014) 325-331.
[7] G. Centi, S. Perathoner, Catal. Today, 148 (2009) 191-205.
[8] K.R. Thampi, J. Kiwi, M. Gratzel, Nature, 327 (1987) 506-508.
[9] P. Sabatier, Making methane or mixtures of methane and hydrogen, Fr. Pat., 1910.
[10] F. Sastre, A.V. Puga, L. Liu, A. Corma, H. García, J. Am. Chem. Soc., 136 (2014) 6798-6801.
[11] X. Meng, T. Wang, L. Liu, S. Ouyang, P. Li, H. Hu, T. Kako, H. Iwai, A. Tanaka, J. Ye, Angew. Chem.-Int. Edit., 53 (2014) 11478-11482.
[12] P.G. O'Brien, A. Sandhel, T.E. Wood, A.A. Jelle, L.B. Hoch, D.D. Perovic, C.A. Mims, G.A. Ozin, Adv. Sci., 1 (2014) DOI: 10.1002/advs.201400001.
[13] A. Dhakshinamoorthy, S. Navalon, A. Corma, H. Garcia, Energy Environ. Sci., 5 (2012) 9217-9233.
[14] Y. Izumi, Coord. Chem. Rev., 257 (2013) 171-186.
[15] V.P. Indrakanti, J.D. Kubicki, H.H. Schobert, Energy Environ. Sci., 2 (2009) 745-758.
[16] Y. Ma, X. Wang, Y. Jia, X. Chen, H. Han, C. Li, Chem. Rev., 114 (2014) 9987-10043.
[17] S. Navalón, A. Dhakshinamoorthy, M. Álvaro, H. Garcia, ChemSusChem, 6 (2013) 562-577.
[18] Slamet, H.W. Nasution, E. Purnama, S. Kosela, J. Gunlazuardi, Catal. Commun., 6 (2005) 313-319.
[19] I.H. Tseng, W.C. Chang, J.C.S. Wu, Appl. Catal. B-Environ., 37 (2002) 37-48.
[20] I.H. Tseng, J.C.S. Wu, Catal. Today, 97 (2004) 113-119.
[21] H. Yamashita, H. Nishiguchi, N. Kamada, M. Anpo, Y. Teraoka, H. Hatano, S. Ehara, K. Kikui, L. Palmisano, A. Sclafani, M. Schiavello, M.A. Fox, Res. Chem. Intermed., 20 (1994) 815-823.
[22] K. Adachi, K. Ohta, T. Mizuno, Sol. Energy, 53 (1994) 187-190.
[23] L. Liu, F. Gao, H. Zhao, Y. Li, Appl. Catal. B-Environ., 134 (2013) 349-358.
[24] K. Hirano, K. Inoue, T. Yatsu, J. Photochem. Photobiol. A-Chem., 64 (1992) 255-258.
[25] C.-C. Yang, Y.-H. Yu, B. van der Linden, J.C.S. Wu, G. Mul, J. Am. Chem. Soc., 132 (2010) 8398-8406.
[26] L. Zhang, P. De Schryver, B. De Gusseme, W. De Muynck, N. Boon, W. Verstraete, Water Res., 42 (2008) 1-12.
[27] R. Priya, S. Kanmani, Environ. Technol., 34 (2013) 2821-2828.
[28] K. Zhang, L. Guo, Catal. Sci. Technol., 3 (2013) 1672-1690.
[29] X.B. Chen, S.H. Shen, L.J. Guo, S.S. Mao, Chem. Rev., 110 (2010) 6503-6570.
[30] W.J. Chung, J.J. Griebel, E.T. Kim, H. Yoon, A.G. Simmonds, H.J. Ji, P.T. Dirlam, R.S. Glass, J.J. Wie, N.A. Nguyen, B.W. Guralnick, J. Park, A. Somogyi, P. Theato, M.E. Mackay, Y.-E. Sung, K. Char, J. Pyun, Nat. Chem., 5 (2013) 518-524.
[31] R.D. Shannon, Acta Crystallogr. Sect. A: Found. Crystallogr., 32 (1976) 751-767.
[32] K. Nagaveni, M.S. Hegde, G. Madras, J. Phys. Chem. B, 108 (2004) 20204-20212.
[33] L.Y. Chen, T. Horiuchi, T. Osaki, T. Mori, Appl. Catal. B-Environ., 23 (1999) 259-269.
[34] S. Velu, K. Suzuki, M. Okazaki, M.P. Kapoor, T. Osaki, F. Ohashi, J. Catal., 194 (2000) 373-384.
[35] H. Praliaud, S. Mikhailenko, Z. Chajar, M. Primet, Appl. Catal. B-Environ., 16 (1998) 359-374.
[36] J.F. Xu, W. Ji, Z.X. Shen, S.H. Tang, X.R. Ye, D.Z. Jia, X.Q. Xin, J. Solid State Chem., 147 (1999) 516-519.

[37] H. Kisch, P. Lutz, Photochem. Photobiol. Sci., 1 (2002) 240-245.
[38] M. Kanemoto, T. Shiragami, C.J. Pac, S. Yanagida, J. Phys. Chem., 96 (1992) 3521-3526.